Lanthanide-Doped Scandia and Yttria Cathodoluminescent Films: A Comparative Study

Daniele Gozzi,*[,†] Alessandro Latini,[†] Daniela Carta,[‡] Anna Corrias,[‡] Andrea Falqui,[‡] Gavin Mountjoy,[§,‡] Laura Lazzarini,[||] Giancarlo Salviati,[||] and Steven G. Fiddy[⊥]

Dipartimento di Chimica, SAPIENZA, Università di Roma, Piazzale Aldo Moro 5, 00185 Roma, Italy, Dipartimento di Scienze Chimiche, Università di Cagliari, Complesso Universitario, S.S. 554 bivio per Sestu, 09042 Monserrato, Cagliari, Italy, IMEM-CNR, Parco Area delle Scienze 37/A, Località Fontanini, 43010 Parma, Italy, and Daresbury Laboratory, Keckwick Lane, Warrington, Cheshire, WA4 4AD, United Kingdom

Received May 23, 2008. Revised Manuscript Received June 20, 2008

A comparative study of red-green-blue cathodoluminescent films based on yttria (Y_2O_3) and scandia (Sc_2O_3) as host materials was carried out. Europia (Eu_2O_3), terbia (Tb_2O_3), and thulia (Tm_2O_3) were used as dopant, respectively, for the red, green, and blue light emissions. The films were grown on quartz optical polished substrates heated at 800 °C by EB-PVD codeposition. EXAFS and XANES spectroscopies were used for determining the local structure around the lanthanide ion, whereas thin film XRD and HREM were employed to characterize the bulk microstructure. For a given dopant and concentration, the light emissions were found to be more intense for films having scandia as host. This was found to be due to a greater asymmetry of the lanthanide dopant caused by the differences in size between the doping and the host ion.

Introduction

Lanthanide-doped oxides yttria (Y_2O_3) and scandia (Sc_2O_3) have been found to be interesting materials for many technological applications in the field of optical devices, such as luminescence displays, optical amplifiers,[1−4] and solid-state lasers.[5] Scandium oxide is a wide band gap (5.7 eV) material with high bulk refractive index ($n = 1.90$ at 400 nm), high physical stability (melting point at 2753 K), as well as very a high chemical stability[6] ($\Delta_f G^{\theta}_{298} = -1818$ kJ mol^{-1}). Because of its large damage threshold to high-power lasers, Sc_2O_3 has been used for high reflectance coatings for UV applications.[7] Because of its high thermal conductivity, trivalent rare-earth-doped scandia is a very suitable host material for high-power solid-state lasers.[8] The crystallographic structure of sesquioxides under normal conditions is the cubic *C*-type bixbyite structure (space group symmetry $Ia\bar{3}$). This structure is stable up to the melting point (~2700 K) for scandia and slightly below it for yttria. The lattice constants are $a_{Sc_2O_3} = 985.7$ pm and $a_{Y_2O_3} = 1060.3$ pm, respectively. A unit cell of the bixbyite structure contains 16 f.u. (80 atoms) with 32 cation sites. Twenty four cation sites of the unit cell have C_2 symmetry (axis of symmetry $\|\langle 100\rangle$ direction) and eight cation sites have C_{3i} symmetry (axis of symmetry $\|\langle 111\rangle$ direction), both 6-fold coordinated with oxygen. Calculations of the effective charges result in higher effective charge of the metal ions in C_{3i} symmetry in comparison with C_2 symmetry.[9]

In a previous study,[10] the growth and characterization of red-green-blue cathodoluminescent films based on yttria (Y_2O_3) and gadolinia (Gd_2O_3) as host materials were studied. Europia (Eu_2O_3), terbia (Tb_2O_3), and thulia (Tm_2O_3) were used as dopant, respectively, for the red, green, and blue light emissions. It was found that doped Y_2O_3 films gave the best performances. Under the same excitation conditions, they showed a more intense luminescence with respect to the doped Gd_2O_3 films. Because of the cubic structure of both host and dopant, doped Y_2O_3 films are physically more stable and their deposition and growth do not require special experimental conditions. However, the poor intensity of the blue luminescence in both hosts was not solved and it is not yet clear what are the key parameters that influence the emission intensity and, if all the other conditions are fixed, what is the role of host. The scope of this work is to find the conditions to improve the emission intensities and to

* Corresponding author. E-mail: daniele.gozzi@uniroma1.it.
† Università di Roma.
‡ Università di Cagliari.
§ Permanent address: School of Physics, University of Kent, Canterbury, UK.
|| IMEM-CNR.
⊥ Daresbury Laboratory.

(1) Blasse, G.; Grabmeier, B. C., *Luminescent Material*;, Springer: Berlin, 1994.
(2) Ronda, C. R. *J. Lumin.* **1997**, *72*, 49.
(3) Brenier, C. R.; Boulon, G. *Europhys. Lett.* **2001**, *55*, 647.
(4) Pradhan, A. K.; Zhang, K.; Mohanty, S.; Dadson, J.; Hunter, D.; Loutts, G. B.; Roy, U. N.; Cui, Y.; Burger, A.; Wilkerson, A. L. *J. Appl. Phys.* **2005**, *97*, 023513.
(5) Peters, R.; Kränkel, C.; Petersmann, K.; Huber, G. *Opt. Express* **2007**, *15*, 7075.
(6) Belov, G. V.; Iorish, V. S.; Yungman, V. S. *IVTANTHERMO for Windows; Database of Thermodynamic Properties of Individual Substances and Thermodynamic Modeling Software*, version 3.0; Glushko Thermocenter of Russian Academy of Sciences: Moscow, Russia, 2005.
(7) Grosso, D.; Sermon, P. A. *Thin Solid Films* **2000**, *368*, 116.
(8) Peters, V.; Mix, E.; Fornasiero, L.; Petersmann, K.; Huber, G.; Basun, S. A. *Laser Phys.* **2000**, *10*, 417.
(9) Xu, Y.; Gu, Z.; Ching, W. Y. *Phys. Rev. B* **1997**, *56*, 14993.
(10) Gozzi, D.; Latini, A.; Salviati, G.; Armani, N. *J. Appl. Phys.* **2006**, *99*, 123524.

10.1021/cm8014176 CCC: $40.75
Published on Web 08/06/2008

Table 1. Composition of Lanthanide-Doped (D) Yttria (Y) and Scandia (S) films as Ratio, r_{dh}, between the Measured Grown Thicknesses of Dopant (d) and Host (h); Below Each Ratio, The Dopant Molar Concentration, c_d, Calculated According to Eq 2, is Reported in Italics[a]

	composition (r_{dh}, c_d)				
EDY	0.101	0.068	0.054	0.049	0.037
	0.087	*0.064*	*0.049*	*0.044*	*0.034*
TDY	0.102	0.077	0.065	0.051	0.032
	0.090	*0.069*	*0.060*	*0.047*	*0.030*
TmDY	0.102	0.077	0.064	0.046	0.036
	0.092	*0.072*	*0.060*	*0.044*	*0.034*
EDS	0.099	0.047			
	0.070	*0.034*			
TDS	0.100	0.052			
	0.071	*0.039*			
TmDS	0.099	0.048			
	0.073	*0.037*			

[a] E, T, and Tm stand, respectively, for Europia (Eu_2O_3), terbia (Tb_2O_3), and thulia (Tm_2O_3).

understand, through the comparison of the scandia with yttria films, the reciprocal host−dopant influence by gathering local structure information using X-ray absoption spectroscopy. This work gives a contribution not only to the optical devices development such as field effect displays (FEDs), waveguiding thin films, and solid-state lasers but also to improving the knowledge on scandia-doped films, which is still very limited.

Experimental Section

The film samples were deposited on $50 \times 20 \times 1$ mm^3 fused silica optically polished substrates by electron beam physical vapor codeposition EB-PVCD of ceramic host and rare-earth oxide. The EB target materials are the pure oxide powders from Aldrich shaped as pellets obtained by room temperature pressing. The EB crucibles are made of TiB_2/BN composite material, which has been tested to be inert toward the oxide pellets. The codeposition has been carried out at 3.5 keV by a Ferrotec Germany double EB gun system through the control of the respective deposition rates by using two independent quartz microbalances. The ratio between the dopant and host is roughly fixed by setting the ratio between the respective deposition rates. This requires setting separately in both the microbalances the density value and acoustic impedance factor of host and dopant oxides. The deposition rate of hosts has been always set at 1.50 nm s^{-1}, and the dopant deposition rate has been adjusted accordingly to the prefixed dopant concentration. Then, by energy dispersion spectroscopy analysis, EDS, the true value of the dopant concentration in the host has been measured. The deposition time has been adjusted each time in order to obtain a growth thickness around 1 μm. Table 1 shows the composition of the studied film samples given as ratio between the thicknesses of dopant and host as grown separately. The thickness values evaluated according to the quartz microbalances were checked by measuring the cross section of some film samples by scanning electron microscopy, SEM. Both data agree satisfactorily. During the deposition, the substrate has been heated to 800 °C by using a high power halogen lamp. The pressure inside the chamber, while deposition is in progress, was always below 1×10^{-5} mbar. Each film has been analyzed by X-ray diffraction, XRD, using the thin film module with graphite monochromator of the X'Pert Pro apparatus by Philips. All the XRD spectra have been carried out by using a Cu anode source filtered by Ni and corrected from the Cu $K\alpha 2$ line according to the ratio Cu $K\alpha 2$/Cu $K\alpha 1$=0.5. The 2θ scan step size was 0.02°.

By using a Gatan MonoCL2 system installed on a Cambridge S-360 SEM coupled with a multialkali photomultiplier detector, we performed the spectrally resolved cathodoluminescence (CL) investigations. The samples were coated by a 10 nm thick gold layer in order to prevent charging effects. Typical experimental conditions for all the samples investigated were electron beam energy of 20 keV, beam current of 3 nA, magnification of 500× and temperature of 300 K.

HREM analysis was carried out using a JEOL JEM2100F transmission electron microscope operating at 200 kV and equipped with a field-emission electron source. To produce the samples for HREM cross-section analysis, 2×2 mm^2 plates were glued together using epoxy in such a way that the film sides faced each other. A mechanical polishing procedure was carried out on all the samples to achieve a 40 μm thickness on the direction parallel to the glass cut. Final thinning to electron transparency was achieved by precision ion milling with two Ar guns at 5 keV (Gatan PIPS).

The X-ray absorption spectroscopy experiments were carried out on station 7.1 of the SRS, Daresbury Laboratory, U.K. Data were collected at room temperature using a Si(111) monochromator at the Eu (6977 eV), Tb (7514 eV), and Tm (8648 eV) L_{III}-edges.

Data on film samples were collected in the fluorescence mode, whereas data on reference samples (Eu_2O_3, Tb_2O_3, and Tm_2O_3) were collected in the transmission mode on powders deposited on polyethylene membranes.

The XANES spectra were processed in the usual way to obtain normalized absorbance. L_{III}-edge XANES represents $p_{3/2} \rightarrow d_{3/2}$ and $d_{5/2}$ transitions. Previous work has shown a clear trend in the main absorption peak of the L_{III}-edge of rare earth oxides when rare earth has valence of 3+. There is one peak at the main absorption edge, and the width of the main peak changes with the site symmetry.[11−14] This has been explained as being due to the crystal field splitting of the d states,[11,14,15] e.g., the splitting is larger and the main peak is broader for a site with octahedral symmetry compared with the tetrahedral symmetry.[11,16]

The XANES spectra have been analyzed qualitatively by comparing spectra from samples with those from reference compounds and looking for differences between yttria and scandia hosts.

The EXAFS data were processed using the program Viper, which was used to sum the data, identify the beginning of the absorption edge, E_o, fit pre- and postedge backgrounds, and hence obtain the normalized absorbance χ as a function of the modulus of the photoelectron wavevector k.[17] The modular package DL_EXCURV,[18] based on the EXCURV98 code, was used in the final stage of data processing to model the experimental $\chi(k)$ in order to extract structural information. This code uses fast curved wave theory[19] and calculates ab initio the effective curved wave backscattering amplitude of the scatterer, the phase shift due to the absorbing atom potential, the phase shift due to the scatterer, and

(11) Antonio, M. R.; Soderholm, L.; Ellison, A. J. G. *J. Alloys Compd.* **1997**, *250*, 536.
(12) Loeffen, P. W.; Pettifor, R. F.; Müllender, S.; van Veenendaal, M. A.; Röhler, J.; Sivia, D. S. *Phys. Rev. B* **1996**, *54*, 14877.
(13) Larson, E. M.; Ellison, A. J. G.; Lytle, F. W.; Navrotsky, A.; Greegor, R. B.; Wong, J. *J. Non-Cryst. Solids* **1991**, *130*, 260.
(14) Pederson, K. R.; Jrgensen, J. E. *Physica C* **1996**, *264*, 185.
(15) Soldatov, A. V.; Ivanchenko, T. S.; Longa, S. D.; Kotani, A.; Iwamoto, Y.; Bianconi, A. *Phys. Rev. B* **1994**, *50*, 5074.
(16) Hilbrig, F.; Göbel, H. E.; Knözinger, H.; Schmelz, H.; Lengeler, B. *J. Phys. Chem.* **1991**, *95*, 6973.
(17) Klementiev, K. V. *Appl. Phys.* **2001**, *34*, 209.
(18) Tomic, S.; Searle, B.G;. Wander, A.; Harrison, N. M.; Dent, A. J.; Mosselmans, J. F. W.; Inglesfield, J. E. *CCLRC Technical Report DL-TR-2005-001, ISSN 1362−0207*; Crown of the Continent Research Learning Center: Warrington, U.K., 2004.
(19) Gurman, S. J.; Binsted, N.; Ross, I. *J. Phys. C* **1984**, *17*, 143.

the mean free path of the photoelectron.[20,21] The k-independent parameter (called AFAC in EXCURV98), which is the many-body amplitude reduction factor, was determined to be 1 from fitting to the reference samples. The parameter EF, which is a correction to E_0, was free to vary in all fittings. The structural parameters were obtained by nonlinear least-squares fitting in k-space with a k^3 weighting of the total experimental EXAFS spectra to emphasize the high-energy part of the spectrum. The fitting was carried out using the k range 2.5−12 Å^{-1}. Fitting was performed introducing only single scattering contributions since multiple scattering on these samples can be neglected up to 4 Å.[22] The errors in the fit parameters, R_i, N_i, and $2s_i^2$ (Debye−Waller factor (DW)), were obtained from the 95% confidence level,[23] as calculated in EXCURV98. The number of fitted parameters was always less than the number of statistically independent data points, as estimated in the standard way.[23] The quality of the fit was judged from the normalized sum of residuals

$$\text{R-factor} = \sum_n k_n^3 |\chi_{\text{expt}}(k_n) - \chi_{\text{fit}}(k_n)| \Big/ \sum_n k_n^3 |\chi_{\text{expt}}(k_n)| \times 100 \quad (1)$$

Reasonable EXAFS fits of single shells typically have R-factor values around 20%; however, when the fit is performed on the total EXAFS spectra, higher values of R-factor can still correspond to good fits, especially if the fit is not extended to peaks at high R.

Results

The cathodoluminescent spectra are reported in Figure 1 at the dopant/host thickness ratio of 0.1. In each panel, the comparison is made between the same dopant in both yttria and scandia hosts. The acronyms XDY and XDS stand for X-doped yttria and X-doped scandia, where X is the rare earth, RE, dopant (X = E = Eu, X = T = Tb, X = Tm). The peak positions are as expected for yttria and scandia hosts and in agreement with CL spectra previously found also in the gadolinia host.[10] On the contrary, the intensity is host depending. From the top to the bottom of Figure 1, the intensity ratios at the respective maxima are 1.5 (611 nm), 7.7 (542 nm), and 1.6 (454 nm). Figures 2 and 3 show the thin film XRD spectra of samples having yttria and scandia hosts, respectively. In each panel of both figures, the reference spectrum of the respective dopant is reported. The features of the XRD spectra are given in Table 2. In the same table, the reference features[24] with their relative intensities are also reported. The XRD spectra were analyzed by MAUD software[25] in order to obtain for each film sample of given dopant/host ratio, r_{dh}, the main and minor orientation of the crystallites and their average size. All these information are summarized in Table 3.

Figure 4 shows, respectively, in panel A and B the trends of the cathodoluminescent spectrum integral (CSI) and the crystallite size, both vs the dopant molar concentration, c_d. The dependency of CSI against the crystallite size is also

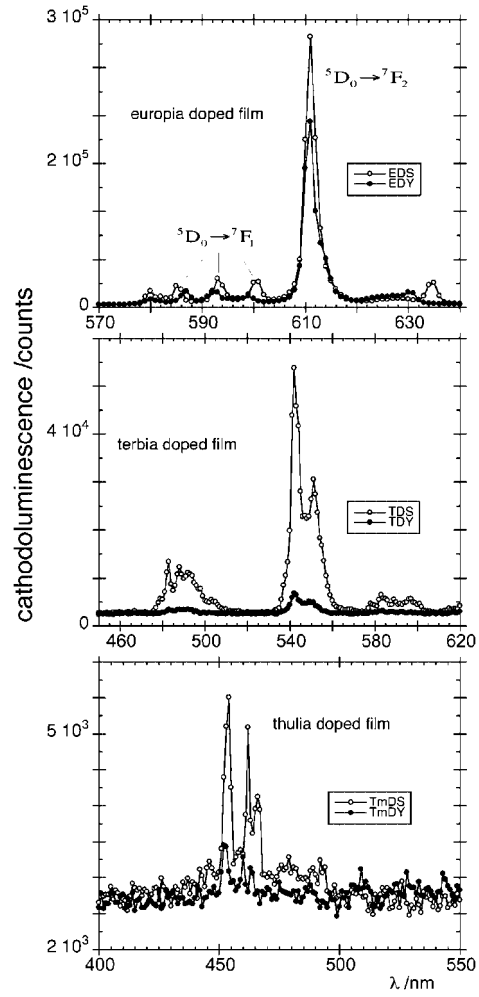

Figure 1. Cathodoluminescence spectra of films at dopant/host thickness ratio of 0.1. Each panel shows the spectra with the same dopant respectively in yttria (Y) and scandia (S) hosts.

reported in panel C. Colored points refer everywhere to the scandia-doped films and black points to yttria-doped films. The interpolated curves serve only to guide the eye.

To pass from r_{dh} to c_d the equation below was used:

$$c_d = r_{dh} f_{dh} / (1 + r_{dh} f_{dh}); \quad f_{dh} = \rho_d M_h / \rho_h M_d \quad (2)$$

where ρ and M are, respectively, the density and molecular weight of dopant (d) or host (h) oxides. The film stoichiometry is $Y_{2-x}RE_xO_3$ and $Sc_{2-x}RE_xO_3$. They are substitution type solid solutions with $x = 2c_d$.

In Figures 5 and 6, the HREM images of the samples having yttria and scandia hosts, respectively, are reported. The samples having yttria host show large regions with preferential growth, as evident in the typical images obtained for samples doped with Eu, Tb, and Tm, where lattice planes with spacing around 0.3 nm are evident, corresponding to 222 planes. The samples having scandia host result to be less oriented, as can be inferred from the HREM images that show regions with different orientation.

In Figure 7, the XANES spectra of Eu_2O_3, Tb_2O_3, and Tm_2O_3 and film samples having yttria and scandia hosts with dopant/host thickness ratio of 0.1 are reported.

Figures 8 and 9 show the EXAFS spectra and the corresponding Fourier Transforms (FTs) of the reference

(20) Von Barth, U.; Hedin, L. *J. Phys. C* **1972**, *5*, 1629.
(21) Crozier, E. D. *Nucl. Instr. Method Phys. Res., Sect. B* **1997**, *133*, 134.
(22) Qi, Z.; Liu, M.; Chen, Y.; Zhang, G.; Xu, M.; Shi, C.; Zhang, W.; Yin, M.; Xie, Y. *J. Phys Chem. C* **2007**, *111*, 1945.
(23) Error Report of the International XAFS Society Standards and Criteria Committee; http://ixs.iit.edu/subcommittee_reports/sc/ (2000).
(24) *JCPDS*; International Centre for Diffraction Data: Chester, U.K., 2001.
(25) Lutterotti, L. *Materials Analysis Using Diffraction, MAUD*, version 2.064, 2008; http://www.ing.unitn.it/~maud/.

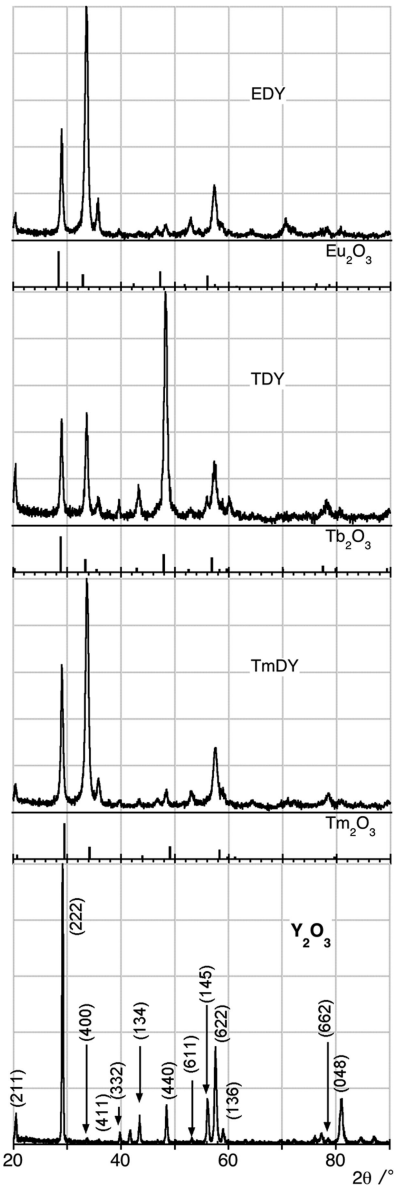

Figure 2. Thin film XRD spectra of films at dopant/host thickness ratio of 0.1. The host is yttria. To each panel is associated the reference JCPDS[24] spectrum of the related dopant. The bottom panel refers to the spectrum of a pure yttria film.

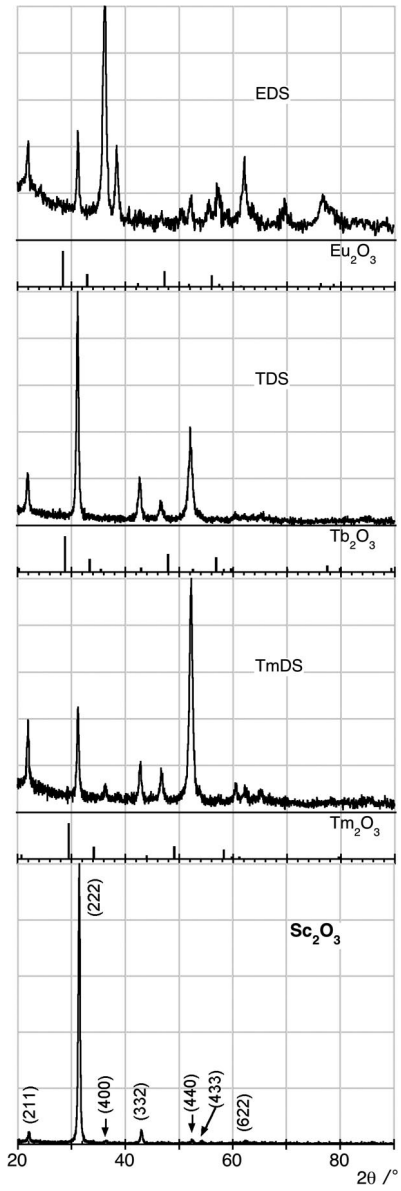

Figure 3. Thin film XRD spectra of films at dopant/host thickness ratio of 0.1. The host is scandia. To each panel is associated the reference JCPDS[24] spectrum of the related dopant. The bottom panel refers to the spectrum of a pure scandia film.

samples as well as yttria and scandia-doped films with dopant/host thickness ratio of 0.1.

Discussion

Looking at Figure 7, a strong similarity between the XANES spectra for Eu_2O_3, Tb_2O_3 and Tm_2O_3 is observed. The slight difference in positions of multiple scattering (MS) peaks at ~25 and ~45 eV above the absorption edges is due to different distances in the structure of the three oxides reflecting changing size of the RE ion (decreasing from Eu to Tb to Tm). The XANES spectra for Tb_2O_3 and Tm_2O_3 look slightly different to the spectra of Eu_2O_3 in the region ~25 eV above the edge, where there is a small MS peak that is less pronounced in Eu_2O_3. This is due to the large Debye−Waller factors in Eu_2O_3 (see EXAFS results), which dampen the MS effect. The difference in height of the main absorption edge peak reflects the available f-electron states at the absorption edge, decreasing with the filling of the f-electron shell from Eu to Tb to Tm.

The XANES spectra of all the samples (Eu, Tb, and Tm) are quite similar to the reference compounds which are consistent with them all having a local structure of the RE_2O_3 crystal. There is a slight difference between samples with Y_2O_3 host (see dotted lines) and Sc_2O_3 host (see solid lines). The difference is of the same type as seen when comparing Eu_2O_3, Tb_2O_3, and Tm_2O_3. The slight difference in positions of MS peaks at ~25 and ~45 eV, above the absorption edges, is due to different distances in the structure reflecting changing size of the ion (decreasing from Y to Sc). There is also a difference in height of the main absorption edge peak, decreasing from Y_2O_3 to Sc_2O_3, but this is not due to the available f-electron states, as there are none available in Y or Sc. Instead, it is correlated with a slight broadening of the main absorption edge peak in Sc_2O_3 compared to Y_2O_3. This indicates a site with slightly lower symmetry in Sc_2O_3

Table 2. XRD Reference Data for Host and Dopant Oxides[a]

	host				dopant					
	Sc_2O_3		Y_2O_3		Eu_2O_3		Tb_2O_3		Tm_2O_3	
cell (*a*, *b*, *c*) (pm)	984.9, 0, 0		1060, 0, 0		1086, 0, 0		1073, 0, 0		1048, 0, 0	
space group	*Ia*$\bar{3}$(206)		*Ia*$\bar{3}$(206)		*Ia*$\bar{3}$(206)		*Ia*$\bar{3}$(206)		*Ia*$\bar{3}$(206)	
lattice	body-centered		body-centered		body-centered		body-centered		body-centered	
system	cubic		cubic		cubic		cubic		cubic	
JCPDS[24] no.	74−1210		82−2415		34−0392		23−1418		41−1090	
intensity	2θ (deg)	*h k l*	2θ (deg)	*h k l*	2θ (deg)	*h k l*	2θ (deg)	*h k l*	2θ (deg)	*h k l*
1st	31.439[1]	2 2 2	29.155[1]	2 2 2	28.421	2 2 2	28.803	2 2 2	29.474	2 2 2
2nd	52.518[4]	4 4 0	48.536[4]	4 4 0	47.266	4 4 0	47.925	4 4 0	49.098	4 4 0
3rd	22.090[3]	2 1 1	33.790[8]	4 0 0	32.926	4 0 0	56.866	6 2 2	34.155	4 0 0
4th	62.503[6]	6 2 2	57.625[2]	6 2 2	56.077	6 2 2	33.381	4 0 0	58.311	6 2 2
5th	36.461[5]	4 0 0	20.503[5]	2 1 1	76.312	6 6 2	77.480	6 6 2	20.712	2 1 1
6th	43.042[2]	3 3 2	43.490[5]	1 3 4	42.362	4 3 1				
7th	*64.072*	*6 3 1*	78.602[8]	6 6 2	78.678	8 4 0				
8th	*47.008*	*1 3 4*	39.849[7]	3 3 2	51.809	6 1 1				
9th	*57.649*	*6 1 1*	59.046[6]	1 3 6	57.453	6 3 1				
10th	*60.911*	*5 4 1*	35.908[8]	4 1 1	61.473	6 4 0				
11th	*38.759*	*4 1 1*	53.215[8]	6 1 1						
12th	*85.973*	*6 6 2*	60.447	4 4 4						
13th	*50.730*	*1 2 5*	56.181[3]	1 4 5						
14th	*70.162*	*7 2 1*	81.061[3]	0 4 8						

[a] Superscript numbers refer to the intensity order found in the spectra of the pure host films reported in Figures 2 and 3. Features lacking in the experimental spectra are reported in italics.

Table 3. Data from the XRD Spectrum Analysis by MAUD Software[25] and the Composition of Each Film

	EDY				
composition (th_d/th_h)	0.101	0.068	0.054	0.049	0.037
orientation	400	400	440[a]	400[b]	400
cell parameter (pm)	1064.97 ± 0.06	1064.40 ± 0.08	1063.5 ± 0.2	1062.2 ± 0.2	1063.7 ± 0.1
crystallite size (nm)	25.8 ± 0.5	24.8 ± 0.4	27.6 ± 0.7	41 ± 2	22.6 ± 0.3
	TDY				
composition (th_d/th_h)	0.102	0.077	0.065	0.051	0.032
orientation	400[b]	400[b]	400	400[b]	400
cell parameter (pm)	1062.1 ± 0.3	1062.3 ± 0.2	1063.2 ± 0.6	1062.5 ± 0.2	1063.30 ± 0.05
crystallite size (nm)	31.8 ± 0.9	42 ± 3	24.8 ± 0.3	39 ± 3	27.1 ± 0.3
	TmDY				
composition (th_d/th_h)	0.102	0.077	0.064	0.046	0.036
orientation	400	400	400	400[b]	400
cell parameter (pm)	1062.38 ± 0.06	1062.11 ± 0.08	1062.3 ± 0.7	1060.3 ± 0.2	1063.1 ± 0.6
crystallite size (nm)	24.5 ± 0.5	24.4 ± 0.3	24.3 ± 0.4	31 ± 2	23.8 ± 0.4

	EDS		TDS		TmDS	
composition (th_d/th_h)	0.099	0.047	0.100	0.052	0.099	0.048
orientation	400	440	440[c]	400	440	440
cell parameter (pm)	991.93 ± 0.09	986.7 ± 0.1	992.2 ± 0.1	990.3 ± 0.1	989.7 ± 0.2	987.7 ± 0.5
crystallite size (nm)	23.3 ± 0.7	39 ± 1	52 ± 8	24 ± 1	30 ± 6	32 ± 1

[a] Main orientation. Minor orientation 400. [b] Main orientation. Minor orientation 440. [c] Main orientation. Minor orientation 222.

compared to Y_2O_3. Very similar results were obtained for the films with different ratio between dopant and host thicknesses.

The EXAFS spectra (see Figure 8) for pure Eu_2O_3, Tb_2O_3, and Tm_2O_3 are all quite similar, in agreement with the similar structure of the three oxides. Tm_2O_3 is slightly different in the region 4−6 Å, as a consequence of the shorter distances in the structure. The latter observation is confirmed by the corresponding FTs (see Figure 9) that show shorter distances for Tm_2O_3.

All the film samples having Y_2O_3 host have very similar EXAFS spectra, irrespective of dopant atom (Eu, Tb or Tm). Also the spectra of the film samples with Sc_2O_3 host are very similar. On the other hand, it is worth noticing the significant differences between samples having Y_2O_3 host and samples having Sc_2O_3 host in the region 4−6 $Å^{-1}$ as shown in the spectra of Figure 8. This is evident in the corresponding FTs (see Figure 9) where the differences are concentrated in the second shell. Very similar results were obtained for the films with different ratio between dopant and host thicknesses.

The data of pure Eu_2O_3, Tb_2O_3, and Tm_2O_3 have been fitted using as starting values the parameters taken from their known structures. Because EXAFS is not able to distinguish between the sites with C_2 symmetry and the sites with C_{3i} symmetry, which are both 6-fold coordinated with oxygen, the fitting was done considering as first shell, one-single shell of RE sites coordinated by 6 oxygen atoms, and the same approach was applied for the further shells. The fitting was performed by allowing only small variations in distances, EF, and Debye−Waller factors, while the coordination numbers were kept fixed. The results of the fitting are reported in Figures 8 and 9 and the fitting parameters in

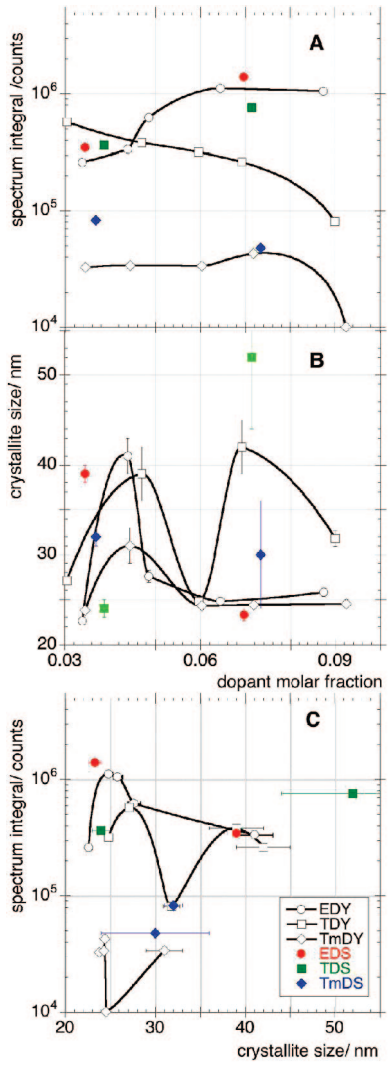

Figure 4. From top to bottom for all the films examined. Colored points refer everywhere to the scandia-doped films and black points to yttria-doped films. The interpolated curves serve only to guide the eye. (A) Integrated cathodoluminescence spectra vs dopant concentration. (B) Crystallite size against dopant concentration. The crystallite size and related error bars were obtained by analyzing the XRD spectra using the MAUD[25] software package. In both panels A and B, the dopant molar concentration was calculated from the thickness ratio dopant/host according to eq 2. (C) Integrated cathodoluminescence spectra vs crystallite size.

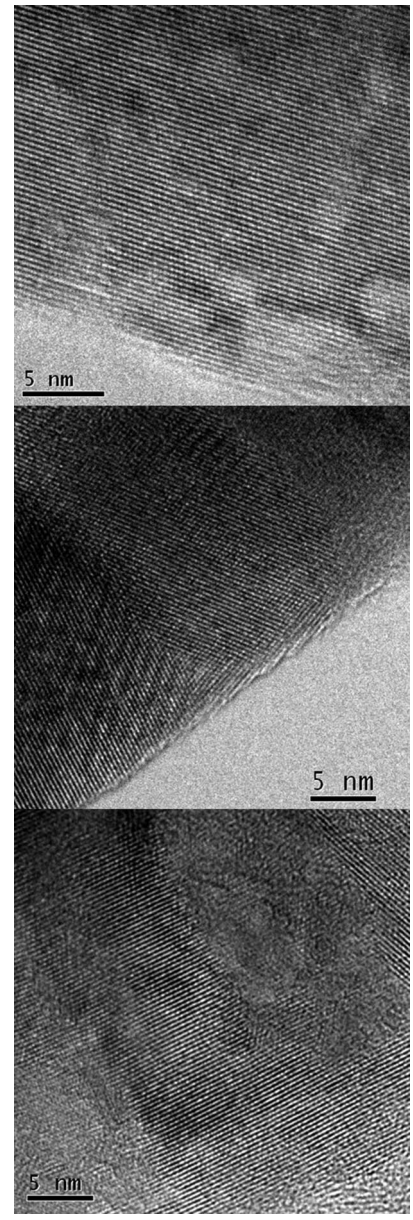

Figure 5. HREM images of films with yttria host having dopant/host thickness ratio of 0.1. From top to bottom: EDY, TDY, TmDY.

Tables 4−6. The fitting results are in agreement with the lattice parameters decreasing in the series Eu_2O_3, Tb_2O_3, Tm_2O_3. Moreover, the Debye−Waller factors for Eu_2O_3 result to be larger than those of Tb_2O_3 and Tm_2O_3.

The fitting of the EXAFS data of all the film samples (see Figures 8 and 9) was done considering a first shell of oxygen atoms, as before, and a second shell constituted by either the doping or host ions. In both films having Y_2O_3 host and Sc_2O_3 host good results were obtained with a second shell of only host ions. These results indicate that the doping ions substitute the host ions in the Y_2O_3 and Sc_2O_3 lattice, respectively. This confirms that the films are substitution solid solutions. The fitting parameters of the examined film samples are reported in Tables 4–6.

The main differences in the fitting results are found between the samples with different host, while only minor differences appear as a function of the doping ion. The differences between samples with Y_2O_3 host and Sc_2O_3 host are clearly due to the difference in size between the doping and the host ion. If we compare the lattice parameters reported in Table 2, it is clear that the size of Eu, Tb, and Tm is more similar to Y size than to Sc, which is the smallest of all these ions. The effect is particularly significant on the second shell distances. In fact, the fitting results indicate that second-shell distances are significantly smaller in all samples having Sc_2O_3 host compared to the samples with Y_2O_3 host. The effect is also detectable in a minor extent in the first shell distances that are again smaller for all the samples with Sc_2O_3 host. In particular, it is very interesting to note that while the Eu−O, Tb−O, and Tm−O distances in samples with Y_2O_3 host are the same as in Eu_2O_3, Tb_2O_3, and Tm_2O_3, in the film samples with Sc_2O_3 host the Eu−O, Tb−O, and Tm−O distances are shorter, indicating that the doping ions are somewhat squashed when they enter into the smaller Sc_2O_3 lattice. Moreover, it can be noted that, within samples with the same host, the distances decreases in the series

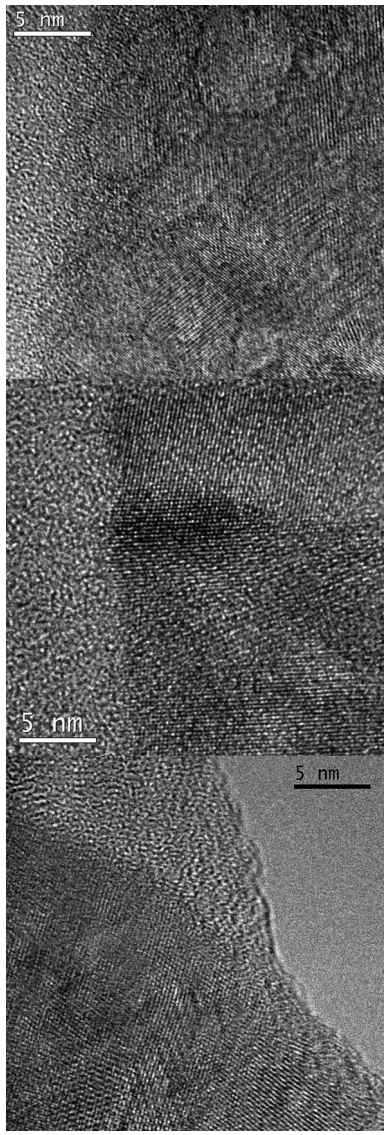

Figure 6. HREM images of films with scandia host host having dopant/host thickness ratio of 0.1. From top to bottom: EDS, TDS, TmDS.

Eu−O, Tb−O, Tm−O, as expected, and the Debye−Waller factors are higher for Eu doped samples, as already observed in the standard oxides.

Through the XANES results, it emerges that the RE sites in Sc_2O_3 have slightly lower symmetry than in Y_2O_3. This is likely associated with the "compression" of the RE ions as it is clearly shown from the EXAFS fitting results. Note that lower symmetry does not necessarily mean larger Debye−Waller factor. The RE−O distances might have a similar spread (in Y_2O_3 and Sc_2O_3), but what is different is the angular arrangement of the oxygens around the RE dopant. This can be understood as a distortion of the symmetry caused by the compression. The lower symmetry of RE dopant sites in Sc_2O_3 host compared to Y_2O_3 host might explain the difference in the optical properties. Alternatively, there is the possibility that the lower symmetry is due to RE cations preferentially occupying the lower symmetry site of the two RE sites. In this case we would expect to observe larger Debye−Waller factors for the film samples having Sc_2O_3 host, and this was not found in the EXAFS results. Considering this, it is more likely that the lower symmetry is due to angular distortion, and not to a larger distribution of RE−O distances.

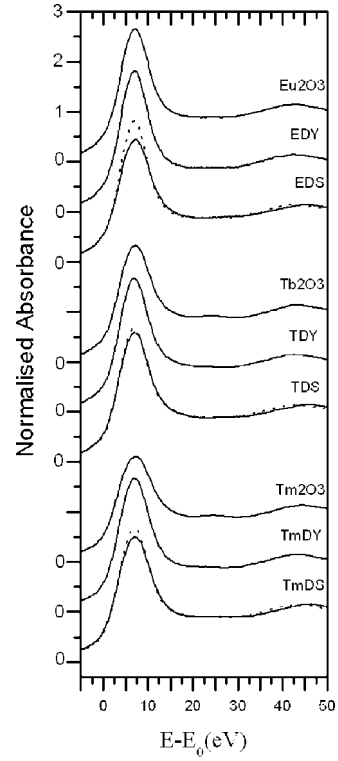

Figure 7. XANES spectra at the Eu, Tb, and Tm L_{III}-edge for standards and for films host having dopant/host thickness ratio of 0.1. The dotted line is the sample with Y_2O_3 host, to help detect the differences between Y_2O_3 and Sc_2O_3 samples.

All the above considerations on the XANES and EXAFS results refer to the local environment of the RE ion in the solid solution with host. Therefore, they are not influenced by the sample microstructure, i.e., crystallite size, grain boundaries, orientation growth, etc. The results coming from XRD and cathodoluminescence spectra refer to average properties of the sample under test and they are also affected by the microstructure. To clarify this aspect, consider the samples with Eu^{3+} in Figure 1 and calculate the ratio, R, between the integral of the electric dipole transition $^5D_0 \rightarrow {}^7F_2$ (from 606 to 619 nm) and the integral of the magnetic dipole $^5D_0 \rightarrow {}^7F_1$ transition. The latter transition is between the $^5D_0$ level and three $^7F_1$ Stark levels (from 583 to 604 nm) of the Eu^{3+} ion in sites of C_2 symmetry.[26,27] The $^5D_0 \rightarrow {}^7F_2$ transition is purely of electric dipole nature and it is very sensitive to the environment of the lanthanide ion; for this reason it is called a hypersensitive transition. In particular, the integrated emission intensity of the $^5D_0 \rightarrow {}^7F_2$transition depends strongly on the site symmetry of the Eu^{3+} ion, differently from that of the $^5D_0 \rightarrow {}^7F_1$ transition, which does not.[28] For these reasons, R is called asymmetry ratio. A high asymmetry ratio value implies that the RE^{3+} ion

(26) Malta, O. L.; Antic-Fidancev, E.; Lemaitre-Blaise, M.; Mililic-Tang, A.; Taibi, M. *J. Alloys Compd.* **1995**, *228*, 41.
(27) Antic-Fidancev, E.; Holsa, J.; Lastusaari, M. *J. Alloys Compd.* **2002**, *341*, 82.
(28) Krsmanovic, R.; Lebedev, O. I.; Speghini, A.; Bettinelli, M.; Polizza, S.; Van Tendeloo, G. *Nanotechnology* **2006**, *17*, 2805.

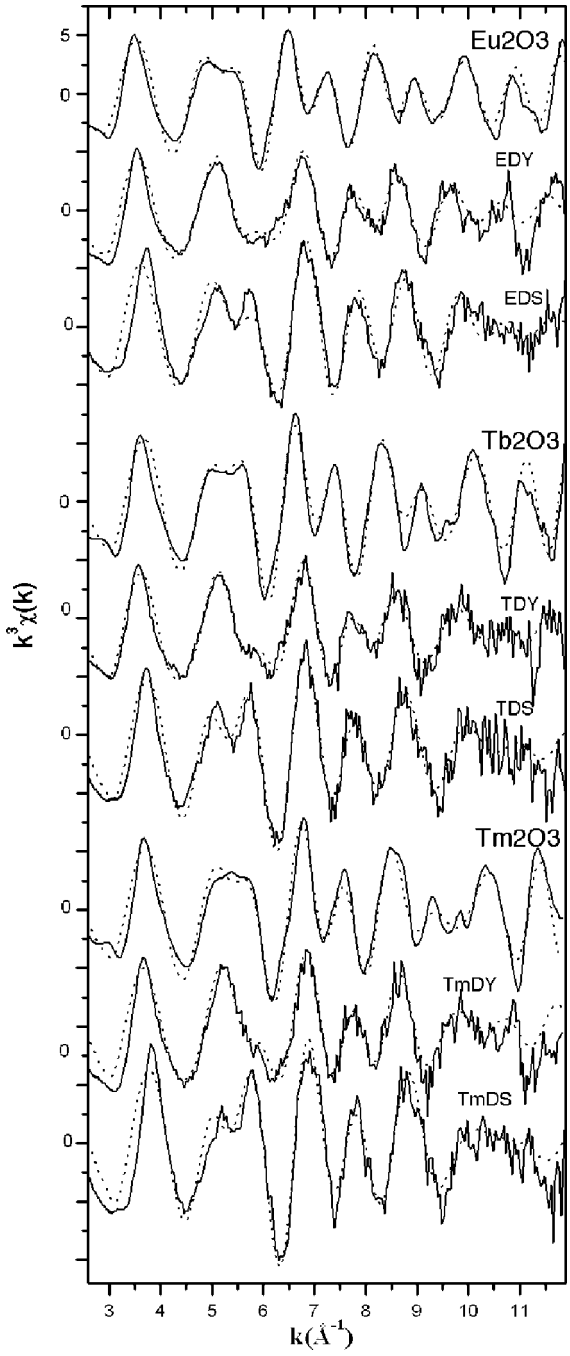

Figure 8. $k^3\chi(k)$ spectra at the Eu, Tb, and Tm L_{III}-edge from experiment (−) and fit results (•••), for standards and for film hosts having a dopant/host thickness ratio of 0.1.

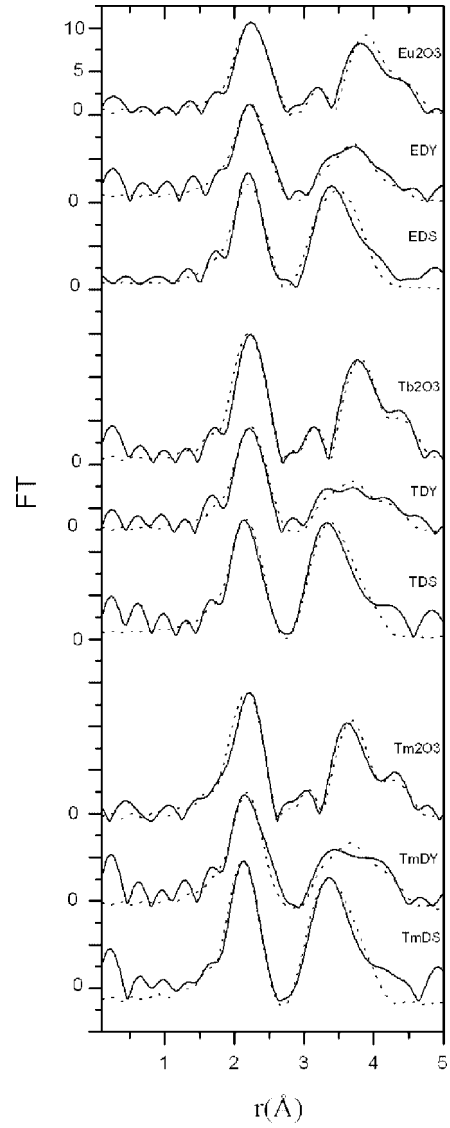

Figure 9. Fourier transforms of $k^3\chi(k)$ spectra at the Eu, Tb, and Tm L_{III}-edge from experiment (−) and fit results (•••), for standards and for film hosts having a dopant/host thickness ratio of 0.1.

Table 4. Interatomic Distances (*R*), Coordination Numbers (N) and Debye−Waller Factors ($2\sigma^2$) Obtained by Fitting the Experimental EXAFS Spectra of Samples Containing Eu

Eu L_{III}-Edge											
	Eu_2O_3				EDY (r_{dh} = 0.101)				EDS (r_{dh} = 0.099)		
	R (Å)	*N*	$2\sigma^2$		*R* (Å)	*N*	$2\sigma^2$		*R* (Å)	*N*	$2\sigma^2$
O	2.33	6	0.021	O	2.33	6	0.021	O	2.30	6	0.021
Eu	3.63	6	0.015	Y	3.57	6	0.021	Sc	3.36	6	0.021
Eu	4.11	6	0.021	Y	4.03	6	0.019	Sc	3.74	6	0.019
	R factor = 27%				*R* factor = 37%				*R* factor = 35%		

is considerably distorted, in agreement with a C_2 symmetry for the sites mainly occupied by the dopant ions. The *R*-values are 3.5 and 3.2 for EDY and EDS, respectively. The value found elsewhere[28] in photoluminescence spectra was 5.3 for EDS nanoparticles doped with 10 mol % Eu_2O_3. According to the EXAFS and XANES evidence, i.e., the lower symmetry of Eu^{3+} sites in the Sc_2O_3 host compared to Y_2O_3 host, the *R* value for EDS should be higher. The above considerations do not take into account that the excited states relax also via another competitive path, which is nonradiative, i.e., phonon emission that quenches light emission. The rate of phonon emission is proportional to exp $(-k\Delta E/h\nu_{max})$ where ΔE is the energy gap to the nearest lower level and $h\nu_{max}$ is the maximum energy of phonons coupled to the emitting states. Fixed the electronic transition, for example the large energy gap transitions $^5D_0 \rightarrow {}^7F_2$ for Eu^{3+} and $^5D_4 \rightarrow {}^7F_5$ for Tb^{3+}, the light intensities of these transitions can be reduced by high values of the $h\nu_{max}$ term. Crystallite size, grain boundaries concentrations, lattice microstrain, impurities, and point defects cause high rate of phonon emission. In the case of films, growth orientation and interaction with substrate have to be also considered. The HREM images

Table 5. Interatomic Distances (R), Coordination Numbers (N), and Debye−Waller Factors ($2\sigma^2$) obtained by Fitting the Experimental EXAFS Spectra of Samples Containing Tb

Tb L_{III}-Edge												
	Tb_2O_3				TDY (r_{dh} = 0.102)				TDS (r_{dh} = 0.100)			
	R (Å)	N	$2\sigma^2$		R (Å)	N	$2\sigma^2$		R (Å)	N	$2\sigma^2$	
O	2.29	6	0.014	O	2.32	6	0.021	O	2.25	6	0.018	
Tb	3.57	6	0.011	Y	3.56	6	0.021	Sc	3.35	6	0.017	
Tb	4.05	6	0.015	Y	4.06	6	0.019	Sc	3.80	6	0.024	
	R factor = 31%				R factor = 32%				R factor = 35%			

Table 6. Interatomic Distances (R), coordination Numbers (N), and Debye−Waller Factors ($2\sigma^2$) Obtained by Fitting the Experimental EXAFS Spectra of Samples Containing Tm

Tm L_{III}-Edge												
	Tm_2O_3				TmDY (r_{dh} = 0.102)				TmDS (r_{dh} = 0.099)			
	R (Å)	N	$2\sigma^2$		R (Å)	N	$2\sigma^2$		R (Å)	N	$2\sigma^2$	
O	2.25	6	0.015	O	2.26	6	0.018	O	2.20	6	0.014	
Tm	3.48	6	0.012	Y	3.53	6	0.020	Sc	3.31	6	0.016	
Tm	3.96	6	0.015	Y	4.00	6	0.025	Sc	3.75	6	0.019	
	R factor = 31%				R factor = 41%				R factor = 40%			

of films with yttria as host show clearly that a preferential growth occurred while no such kind of evidence was found in doped scandia film. The most frequent orientations, as displayed by the thin film XRD spectra of Figures 2 and 3 (see also Table 3), were found to be (400) in doped yttria and (440) in scandia films. The HREM images of films with yttria always show the (222) lattice planes, instead of the (400) which XRD showed to be the main orientation of growth. There are several factors why XRD and HREM give different results. First of all, because the silica substrate is not oriented, the direction of the HREM observation is not easily related to the substrate surface and therefore to the orientation of growth. Second, even if (400) is a preferred orientation, it is not the case that every single grain has this orientation. Moreover, the (222) lattice planes are more visible than (400) planes, because (222) is a more intense reflection, and the (222) lattice planes have a larger spacing.

Because the XRD spectra of both pure host films have a regular pattern, one should infer that the oriented growth is favored by the formation of the solid solutions, $Y_{2-x}RE_xO_3$ and $Sc_{2-x}RE_x\ O_3$. In a previous work,[10] the $Y_{2-x}RE_xO_3$ films with RE = Eu, Tb, Tm, grew (222) oriented though the same experimental growth conditions were adopted with the only exception that the optical polished quartz substrate belonged to a different batch. In that case, the cathodoluminescence intensities were found 4 times higher.

The inspection of the panels of Figure 4 from A to C supports the above arguments. In fact, at same c_d the CSI is always higher for scandia films that have, in general, also larger crystallites but larger crystallites do not ensure intense light emissions. The behavior of TmDY and TmDS films is particularly interesting. The CSI of the former films is practically independent by the dopant concentration except at the highest values where the emission decreases abruptly. By changing c_d, no significant changes are observed in the crystallite size that is around 27 nm throughout the explored interval of thulia concentration. To this almost constant series of values, significant different CSI values correspond. Therefore, other factors related to the microstructure contribute to the nonradiative emission. It is expected that a better correlation with microstructure could be found if oriented substrates were used. It is, however, important to underline the most intense emission of TmDS films with respect to the TmDY emission found in the present work and in the past.[10] The highest intensity observed in the scandia host of the $^1G_4 \rightarrow {}^3H_6$ transition of thulia is clearly shown in Figure 1 (bottom panel). This is important because it is well-known that in the RGB phosphor applications the weak intensity of the blue emission is still a problem. Anyway, it is also worth noticing the large enhancement of all $^5D_4 \rightarrow {}^7F_i$ transitions (with i = 6, 5, 4, 3 and, particularly, the transition with i = 5) of the green emission of terbia when hosted in scandia.

Conclusions

The comparative study reported in this contribution shows the evidence that the lanthanide-doped scandia films are more efficient light emitters than lanthanide-doped yttria films under the same electron beam excitation. The main scope of this paper was also to go inside the physical reasons why this emission enhancement occurs. This was made possible by the synchrotron radiation spectroscopies and through the comparison of the local structures around the RE^{3+} ion hosted in yttria or scandia. The role of the film microstructure in reducing the light emission path in favor of the nonradiative path has been supported on the basis of some experimental evidence.

Acknowledgment. This work has been carried out within the framework of the project "Growth and physico-chemical characterization of films of metallic and ceramic materials" by the working groups of Rome and Cagliari, both funded through the PRIN 2004 call of the Italian Ministry for University and Research. STFC Daresbury Laboratory is acknowledged for the provision of synchrotron radiation, which was supported by the European Community-Access of Research Infrastructure action of the Improving Human Potential Program.

CM8014176